HHS Public Access

Author manuscript

Magn Reson Med. Author manuscript; available in PMC 2020 September 01.

Published in final edited form as:

Magn Reson Med. 2019 September ; 82(3): 1129–1139. doi:10.1002/mrm.27788.

Vessel-specific Quantification of Neonatal Cerebral Venous Oxygenation

Dengrong Jiang[1,2], **Hanzhang Lu**[1,2,3], **Charlamaine Parkinson**[4,5], **Pan Su**[1], **Zhiliang Wei**[1,3], **Li Pan**[1,6], **Aylin Tekes**[1,4], **Thierry A.G.M. Huisman**[1,4], **W. Christopher Golden**[4,5], **Peiying Liu**[1]

[1]The Russell H. Morgan Department of Radiology & Radiological Science, Johns Hopkins University School of Medicine, Baltimore, Maryland, USA.

[2]Department of Biomedical Engineering, Johns Hopkins University School of Medicine, Baltimore, Maryland, USA.

[3]F.M. Kirby Research Center for Functional Brain Imaging, Kennedy Krieger Research Institute, Baltimore, Maryland, USA.

[4]Neurosciences Intensive Care Nursery, Johns Hopkins School of Medicine, Baltimore, Maryland, USA.

[5]Department of Pediatrics, Johns Hopkins School of Medicine, Baltimore, Maryland, USA.

[6]Siemens Healthineers, Baltimore, Maryland, USA.

Abstract

Purpose: Non-invasive measurement of cerebral venous oxygenation (Y_v) in neonates is important in the assessment of brain oxygen extraction and consumption, and may be useful in characterizing brain development and neonatal brain diseases. This study aims to develop a rapid method for vessel-specific measurement of Y_v in neonates.

Methods: We developed a pulse sequence, named accelerated T_2-relaxation-under-phase-contrast (aTRUPC), which consists of velocity-encoding phase-contrast module to isolate pure blood signal, flow-insensitive T_2-preparation to quantify blood T_2, and turbo-field-echo (TFE) scheme for rapid image acquisition, which is critical for neonatal MRI. A series of studies were conducted. First, the pulse sequence was optimized in terms of TFE factor, velocity encoding (VENC), and slice thickness for best sensitivity. Second, to account for the influence of TFE acquisition on T_2 quantification, simulation and experiments were conducted to establish the relationship between TFE-T_2 and standard T_2. Finally, the complete aTRUPC sequence was applied on a group of healthy neonates and normative Y_v values were determined.

Results: Optimal parameters of aTRUPC in neonates were found to be a TFE factor of 15, VENC of 5cm/s, and slice thickness of 10mm. TFE-T_2 was on average 3.9% lower than standard

Corresponding author: Peiying Liu, Ph.D., The Russell H. Morgan Department of Radiology & Radiological Science, Johns Hopkins University School of Medicine, 600 N. Wolfe Street, Park 324, Baltimore, MD 21287, peiying.liu@jhu.edu, Phone: 410-955-4173, Fax: 410-614-1977.

Supporting Information

Supporting Information includes subsections on (1) Calculation of variable FA; (2) Comparison of variable and constant FA; (3) Eddy current correction.

T_2. These two measures were strongly correlated (R^2=0.86), thus their difference can be accounted for by a correction equation, $T_{2,standard}=1.2002\times T_{2,TFE}-10.6276$. Neonatal Y_v values in veins draining cortical brain and those draining central brain were 64.8±2.9% and 70.2±3.3%, respectively, with a significant difference (P=0.02).

Conclusion: aTRUPC MRI has the potential to provide vessel-specific quantification of cerebral Y_v in neonates.

Keywords

Neonates; cerebral venous oxygenation; oxygen consumption; deep venous system; aTRUPC; TRUST

INTRODUCTION

Cerebral oxygenation and metabolism play a critical role during the early stages of brain development. Disruption of oxygen supply and metabolism in neonates is highly detrimental, and has been associated with various diseases such as hypoxic-ischemic encephalopathy (HIE) (1,2) and cerebral stroke (3). Therefore, quantitative measurements of cerebral venous oxygenation (Y_v) in neonates, when combined with arterial oxygenation (Y_a) measured by well-established techniques such as pulse oximetry, may add valuable information to the diagnosis of neonatal brain diseases and to the evaluation of treatments.

Measurement of Y_v in neonates is particularly challenging (4). Positron Emission Tomography (PET) with ^{15}O-labeled radiotracers is considered the gold standard to measure cerebral oxygenation and metabolism in adults (5). However, the application of ^{15}O-PET in neonates (6) is very limited due to its invasive nature, the need of an onsite cyclotron, and in particular the radiation exposure to neonates. Near-infrared spectroscopy (NIRS) is a non-invasive tool that has been successfully used to probe blood oxygenation in neonates (7–9). Although this technique has the advantages of low-cost and the ability for bedside monitoring, a drawback is that the blood oxygenation is usually provided as a relative index instead of in absolute physiological units. Moreover, the application of this optical method is impeded by the penetration depth of light, which makes it particularly difficult to probe oxygenation in deep brain tissues.

In recent years, several MRI-based methods have been employed to provide absolute quantification of Y_v in neonates (10–12). T_2-relaxation-under-spin-tagging (TRUST) is a T_2-based method to quantify global Y_v that has been utilized in healthy neonates (11) as well as in neonates with congenital heart disease (CHD) (13), HIE (14) and punctate white matter lesions (PWML) (15). Another T_2-based technique, termed T_2 prepared tissue relaxation inversion recovery (T2-TRIR), has been shown to be feasible to assess global Y_v in both healthy and HIE neonates (12). A susceptibility-based method, phase-contrast MR susceptometry, has also been utilized to measure global Y_v in neonates with CHD (10). However, despite their successful applications in neonates, all of these MRI techniques provided only an assessment of global Y_v level, which lacks spatial information.

Regional measurement of Y_v in the neonatal brain is of particular clinical importance because early brain development is known to be heterogeneous (16–18) and deep brain regions are more susceptible to injuries (2,19). T_2-relaxation-under-phase-contrast (TRUPC) is a T_2-based MRI technique to quantify Y_v in specific brain vessels and has shown promises in adult population (20,21). However, the long scan time of TRUPC (over 19min when configured for spatial resolution necessary for neonates), is the main obstacle to its application in neonates.

The goal of the present work was to develop a substantially accelerated TRUPC sequence, termed aTRUPC, to obtain vessel-specific Y_v measurement in neonates. A series of studies were conducted. First, the pulse sequence was optimized in terms of turbo-field-echo (TFE) factor, velocity encoding (VENC), and slice thickness for best sensitivity. Second, to account for the influence of TFE acquisition on T_2 quantification, simulation and experiments were conducted to establish the relationship between TFE-T_2 and standard T_2. Finally, the complete aTRUPC sequence was applied on a group of healthy neonates and normative Y_v values were determined, providing for the first time the ability to measure central brain Y_v in addition to cortical brain Y_v. The neonatal Y_v measured by aTRUPC was also validated by comparing it to global Y_v measured with TRUST MRI.

METHODS

Pulse sequence

The proposed aTRUPC pulse sequence is shown in Figure 1a. As can be seen, the sequence is based on the combination of T_2-preparation (red box) and phase-contrast MRI (green box). The phase contrast module allows the isolation of flowing blood signal from surrounding static tissues, and the T_2-preparation module modulates T_2-weighting of the blood signal. With this sequence, two complex images, one phase reference image and a velocity-encoded image, are acquired in an interleaved manner. Complex subtraction of these two images yields a complex difference (CD) image, in which signals from the static tissues are cancelled out and only the signal of flowing blood is present. Non-slice-selective T_2-preparation pulses with varying numbers, characterized by effective TE (eTE), are applied to modulate the T_2-weighting of the blood signal. In post-processing, monoexponential fitting of the blood signal as a function of eTE yields the blood T_2. To remove spin history, post-saturation pulses (blue box) are applied after the last phase-contrast acquisition module (20). One dummy TR is played out before the first acquisition TR to make the magnetization reach steady state.

The major difference between aTRUPC and the original TRUPC sequence is that the original TRUPC acquires only one k-space line per TR; in other words, there is only one phase-contrast acquisition module after each T_2-preparation. Although this design ensures the accuracy of T_2 estimation as the signal is determined solely by the T_2 preparation, it requires long scan time (over 19 minutes for spatial resolution necessary for neonatal scan) to acquire a T_2 map. This is especially limiting for neonates who are susceptible to motion. In contrast, aTRUPC uses a TFE scheme to acquire multiple k-space lines per TR, thus significantly reducing the scan time. A train of phase-contrast acquisition modules (indicated by multiple green boxes in Figure 1a) is applied after each T_2-preparation, and the number

of acquisition modules is referred to as TFE factor. RF spoiling is used to avoid interference among acquisition modules.

Although the use of the TFE scheme drastically reduces the scan time, bias in T_2 estimation can be induced in aTRUPC because the T_2-prepation effect is dissipated later in the acquisition train. Therefore, two strategies were implemented to minimize potential bias in T_2 estimation and image blurring owing to the prolonged acquisition train. First, centric view ordering was employed in aTRUPC acquisition such that the central k-space, which vastly determines the image contrast, is acquired immediately after T_2-preparation, whereas the peripheral k-space is sampled later in the acquisition train (22). Figure 1b shows an example of the view ordering scheme on a 2D k-space. Second, a variable flip angle (FA) scheme (23,24) was applied to reduce signal alteration across the acquisition train. In this work, by assuming a neonatal blood T_1 of 1800ms and T_2 of 70ms (25), the FAs are designed to keep the blood signal constant throughout the acquisition train, for given sequence parameters of recovery time (RT), eTE, and the interval between excitation pulses of two consecutive acquisition modules (hereafter referred to as shot-spacing). As illustrated in Figure 1c, the variable FA series are different among the eTEs, however, the first FA of the series is the same across eTEs so that the signal at the k-space center is solely determined by T_2-preparation. More details of the variable FA scheme, in comparison with traditional constant FA scheme, are shown in Supporting Information and Supporting Information Figure S1.

General experimental methods

A total of eight healthy neonates (5 females and 3 males) were enrolled in this work (for neonatal scans in Study 1 and 3). Note that, compared to neonatal patients, it is considerably more difficult to enroll healthy neonates of several days old, on whom the MRI was performed for research purpose only. Thus, when scan time allowed, some of the participants were used in multiple sub-studies. All neonates were recruited from the Newborn Nursery at Johns Hopkins Children's Center. The neonatal study protocol was approved by the Johns Hopkins University Institutional Review Board. The parents of the neonates gave written informed consent before participating in the study. The gestational age of the recruited neonates at birth was 39.5±0.7 weeks, ranging from 38.4 to 40.4 weeks. The postnatal age at the time of the study was 2.0±1.1 days, ranging from 1 to 4 days. The recruited neonates had no perinatal depression at birth, no known or suspected congenital anatomic or chromosomal anomalies, no major CHD or congenital infection, and no intrauterine drug exposure. Review of the MRI scans by experienced pediatric neuroradiologists confirmed the absence of structural or signal abnormality in the sampled neonates.

All neonatal studies were performed on a 3T Siemens Skyra system (Siemens Healthcare, Erlangen, Germany) using a body coil for radiofrequency transmission and a 20-channel head-neck coil for signal reception, which is the standard clinical setup of neonatal neuroimaging at our institute. The neonates were scanned in natural sleep enhanced by feeding them prior to the imaging study and tightly swaddling the neonates in warmed blankets. Neonatal Noise Guards (MiniMuffs, Natus Pediatrics, Natus Medical Inc., San

Carlos, CA) were used to reduce noise. Foam padding was placed around the head to minimize motion during MRI acquisition. Heart rate and arterial oxygen saturation were monitored via pulse oximetry (Invivo Corporation, Gainesville, USA) throughout the MRI scan. No sedation was used.

In addition to the neonates, eight healthy adult volunteers (25.9±3.3 years old, 4 females and 4 males) were examined (Study 2) and were scanned on a 3T Siemens Prisma system (Siemens Healthcare, Erlangen, Germany) with a 32-channel head coil, after written informed consents were obtained. The adult study protocol was approved by the Johns Hopkins University Institutional Review Board.

In this work, the aTRUPC images were acquired in the mid-sagittal plane given its abundant and well-known venous structures, the flow-encoding direction was anterior-to-posterior matching the predominant anterior-posterior venous blood flow on the mid-sagittal plane (20,21).

Study 1: Optimization of aTRUPC protocol in neonates

Before the full aTRUPC sequence, which consists of acquisitions using three different T_2-preparation durations (eTEs), was applied, we first sought to optimize the key parameters of the sequence in order to obtain the highest sensitivity in unit time, i.e. signal-to-noise ratio (SNR) efficiency. Thus the experiments in Study 1 were performed with eTE=0ms only. Three sequence parameters, specifically TFE factor, slice thickness and VENC, were examined.

To determine the optimal TFE factor, TFE factors of 5, 10 and 15 were tested on 6 neonates (age at birth: 39.6±0.6 weeks, postnatal age: 2.0±1.1 days, 3 females and 3 males). Other imaging parameters included: field of view (FOV)=130×130mm^2, acquisition matrix=256 (foot-to-head, readout direction) × 90 (anterior-to-posterior, phase-encoding direction), RT=1000ms, shot-spacing=17.76ms, slice thickness=10mm, VENC=5cm/s, TE=13.7ms. The number of repetitions was 5, 8 and 10 for the three TFE factors, respectively. The duration was similar across the three scans, which was approximately 3min.

In 5 neonates (age at birth: 39.7±0.6 weeks, postnatal age: 1.6±0.5 days, 3 females and 2 males), we performed aTRUPC-eTE0 sequence using two different slice thicknesses, 5 and 10mm. Other imaging parameters were: TFE factor=15, VENC=5cm/s, TE=13.7ms, 4 repetitions, with a scan time of 72s for each sequence.

In 8 neonates we performed aTRUPC-eTE0 sequence using four different VENCs, 3, 5, 7 and 9cm/s. Data from one neonate was not usable due to excessive motion, so only 7 neonates (age at birth: 39.4±0.6 weeks, postnatal age: 2.1±1.1 days, 4 females and 3 males) were include. Other imaging parameters were: TFE factor=15, slice thickness=10mm, 3 repetitions, and scan time was 54s for each sequence. The minimal allowable TE was used and it was different for different VENC, which was 16.5, 13.7, 12.2 and 11.2ms for the four VENCs, respectively.

Study 2: Relationship between TFE-T_2 and standard T_2

To understand the influence of TFE acquisition scheme on the quantification of blood T_2, numerical Bloch simulations were conducted. In these simulations, signal evolutions along the TFE acquisition train were computed using Bloch equations based on T_1 and T_2 with the optimized TFE factor, and then used to construct k-spaces at different eTEs based on the centric view ordering k-space sampling scheme. Images at different eTEs were reconstructed from corresponding k-spaces and were subsequently used to fit for T_2. Two sets of simulations were performed to investigate how the T_2 bias is dependent on the actual T_1 and T_2 of the blood. In one simulation, we fixed T_1 at 1800ms and varied T_2 from 30 to 115ms. In another simulation, we fixed T_2 at 70ms and varied T_1 from 900 to 2600ms.

Next, we performed a set of experiments to establish the relationship between TFE-T_2 and standard T_2. Due to the long scan duration necessary to collect these data (mainly for the standard T_2 scan), the scans were performed in healthy adults (N=8, aged 25.9±3.3 years old). In each participant, both aTRUPC and the original TRUPC sequences were performed. The common imaging parameters were: FOV=200×200mm^2, acquisition matrix=256 (foot-to-head, readout direction) × 90 (anterior-to-posterior, phase-encoding direction), mid-sagittal slice with 10mm thickness, three eTEs (0, 40 and 80ms) for T_2 quantification, VENC=15cm/s, and flow-encoding direction was anterior-to-posterior. For aTRUPC, additional parameters were: TFE factor=15, variable FAs, RT=1000ms, shot-spacing=17.76ms. For original TRPUC, RT=460ms and FA=90° were used (21). To increase the reliability of the T_2 measurements, each sequence was repeated 8 times in an interleaved manner, resulting in a total scan time of 38min 24s and 7min 28s for original TRUPC and aTRUPC, respectively.

Study 3: Venous oxygenation mapping in neonates

The complete aTRUPC sequence, including all eTEs, was performed in four neonates (age at birth: 39.8±0.6 weeks, postnatal age: 1.5±0.6 days, 2 females and 2 males). The sequence was performed using parameters determined in the optimization study, and three eTEs (0, 40 and 80ms) with 4 repetitions were employed. Scan time of aTRUPC MRI was 3min 44s. For validation purpose, Y_v measured by aTRUPC at the posterior superior sagittal sinus (SSS) was compared to that measured by a global technique, TRUST MRI (11,13–15). The TRUST sequence used parameters established previously (15): imaging slice was positioned 10mm above the sinus confluence, TR=3000ms, TE=8.3ms, TI=1020ms; FOV=160×160×5mm^3, voxel size=2.5×2.5×5mm^3; labeling slab thickness=65mm; 4 eTEs: 0, 40, 80 and 160ms, scan time=1.2min.

Data analysis

The original TRUPC and aTRUPC images were reconstructed with in-house MATLAB (Mathworks, Natick, MA) scripts. Phase artifacts induced by eddy current were corrected as previously described (21), which were detailed in Supporting Information. Motion correction between the images was performed using the FSL FLIRT tool (26).

For Study 1, blood signal in the CD images at eTE=0ms was quantified on a region of interest (ROI) level. Six preliminary ROIs were drawn on the major cerebral veins: three

ROIs on SSS, one ROI on straight sinus (SS), one on the vein of Galen and one on internal cerebral veins. Within each ROI, voxels with the highest signal intensities in the mean CD image were selected as the final mask for this ROI. Due to the different vessel sizes, for the 3 ROIs on the SSS, the top 100 voxels were selected as the final mask; for the other 3 ROIs on SS, vein of Galen and internal cerebral veins, the top 40 voxels were used. For each ROI, an SNR efficiency was quantified on the CD image using the blood/tissue signal ratio divided by the square root of scan time of each repetition, in which the blood signal was the averaged signal intensity in the final mask of the ROI and the tissue signal was quantified as the averaged signal intensity in a rectangular tissue region of 1000 voxels void of discernible vessels. The SNR efficiency was averaged across all ROIs for each neonate and then compared between different protocols.

For Study 2, six ROIs were delineated as described in Study 1 and averaged signals in each ROI were fitted to a monoexponential function of eTE to obtain blood T_2. The T_2 measurements across repetitions were averaged. To establish the relationship between TFE-T_2 and standard T_2, linear regression analysis was performed between these measurements and a conversion equation was calculated. To take into account the uncertainties in both standard T_2 and TFE-T_2 measurements, linear regression was performed by minimizing a modified χ^2 function given by (27):

$$\chi^2_{\mathrm{m}} = \sum_{\mathrm{ROIs}} \frac{\left[T_{2,\,\mathrm{standard}} - \left(\alpha T_{2,\,\mathrm{TFE}} + \beta\right)\right]^2}{\sigma^2_{\mathrm{standard}} + \alpha^2 \sigma^2_{\mathrm{TFE}}} \quad [1]$$

where $T_{2,\mathrm{standard}}$ is the standard T_2 value of one ROI in one subject averaged across repetitions, and $T_{2,\mathrm{TFE}}$ is the corresponding TFE-T_2 estimated by aTRUPC. $\sigma_{\mathrm{standard}}$ and σ_{TFE} are the standard deviations of standard T_2 and TFE-T_2 across repetitions, respectively. α and β are the fitted slope and intercept, and the summation is across all ROIs in all subjects.

For Study 3, both ROI analysis and voxel-wise Y_v mapping were performed. For the ROI analysis, blood TFE-T_2 value was first obtained using a procedure similar to that described in Study 2. The TFE-T_2 was then converted to standard T_2 using the relationship obtained in Study 2. Y_v was then estimated from the T_2 based on a neonate-specific T_2-Y calibration plot established previously (25). The hematocrit of the neonates was assumed to be 0.42 based on the mean hematocrit level of neonatal blood samples reported in (25). For voxel-wise Y_v mapping, a preliminary mask was first manually drawn to encompass the major cerebral veins (SSS, SS, vein of Galen and internal cerebral vein). Median signal intensity in the preliminary mask was determined and 80% of the median was used as a threshold to delineate the final mask. To improve signal stability, signals within the final mask were smoothed by a 9×9 voxel kernel. T_2 fitting was then performed on each voxel within the mask, and the TFE-T_2 was converted to standard T_2 and Y_v, similar to the ROI analysis. The TRUST data analysis followed previous studies (11,13–15). TRUST Y_v at posterior SSS was obtained from each neonate and compared with aTRUPC Y_v measured at posterior SSS.

Statistical analysis

For Study 1, paired t-test was performed to compare SNR efficiency across different imaging protocols. For Study 2, linear regression analysis was performed between TFE-T_2 and standard T_2. For Study 3, mean and standard deviation values of Y_v in each ROI were computed across subjects. To compare Y_v between cortical and central brain regions, values in corresponding ROIs were averaged and then compared using paired t-tests. A $P<0.05$ was considered statistically significant.

RESULTS

Study 1: Optimization of aTRUPC protocol in neonates

Figure 2a illustrates the CD image of a representative neonatal subject and the locations of the six ROIs. Figure 2b shows the comparison between different TFE factors across 6 neonates. It was found that TFE factor of 15 had highest SNR efficiency compared to TFE factor of 5 ($P=0.0004$) and 10 ($P=0.004$). TFE factor of 10 had higher SNR efficiency than TFE factor of 5 ($P=0.001$). Thus TFE factor of 15 was used in the remainder of this work.

Figure 2c shows the comparison between different slice thicknesses across 5 neonates. It was found that slice thickness of 10mm had higher SNR efficiency than that of 5mm ($P=0.04$). Therefore, a slice thickness of 10mm was used in later studies.

Figure 2d shows the comparisons among different VENCs across 7 subjects. VENC of 5cm/s showed significantly higher SNR efficiency than those of 7cm/s ($P=0.04$) and 9cm/s ($P=0.003$). It was also slightly higher than VENC of 3cm/s, although the difference did not reach significance ($P=0.15$). Therefore, a VENC of 5cm/s was considered optimal.

The heart rate and arterial oxygen saturation of the neonates during the MRI scans were 129.8±12.0 beats per minute and 97.9±1.5%, respectively. The results of Study 1 are also summarized in Supporting Information Table S1.

Study 2: Relationship between TFE-T_2 and standard T_2

Simulation results of the differences between TFE-T_2 and standard T_2 are shown in Figure 3. It can be seen that the differences are more sensitive to T_2 than to T_1. The differences varied between −1ms and 2.5ms for typical T_2 values within the physiological range (Figure 3a). On the other hand, the difference dependent on T_1 variation was less than 0.5ms, and was practically negligible within the typical physiologically range of 1400–2400ms (Figure 3b).

Figure 4 shows the experimental results of a scatter plot between the TFE-T_2 obtained from aTRUPC and the standard T_2 obtained from original TRUPC in adults. A strong linear correlation was found between these measurements. Linear fitting resulted in the following relationship between them:

$$T_{2,\,\text{standard}} = 1.2002 \times T_{2,\,\text{TFE}} - 10.6276 \quad [2]$$

where $T_{2,TFE}$ is the TFE-T_2 estimated by aTRUPC, and $T_{2,standard}$ is the standard T_2 value. Henceforth, Equation 2 can be used to convert TFE-T_2 to standard T_2 before applying the T_2-Y calibration curve (25) to estimate Y_v.

Study 3: Venous oxygenation mapping in neonates

Complete aTRUPC sequence was applied on 4 neonates using the sequence parameters optimized in Study 1, i.e. TFE=15, slice thickness=10mm, VENC=5cm/s. Figure 5a shows the CD images of each eTE acquired with aTRUPC in a representative neonate. Figure 5b plots the blood signal in each ROI (yellow arrows in Fig. 5a) as a mono-exponential function of eTEs. The decay rate of the curve yielded TFE-T_2 of the blood, which was corrected using Equation 2 and then converted to Y_v through the neonate-specific T_2-Y calibration plot (Figure 5c). Straight sinus (ROI #4) shows low signal intensity in Figure 5b. Repeated one-way analysis of variance (ANOVA) including all 8 neonates revealed that the SNR efficiency was ROI-dependent (P=0.0001) and was lowest in the straight sinus.

Figure 6a summarizes the group-averaged Y_v values of each ROI. Neonatal Y_v values in veins draining cortical brain (when averaging ROI #1–3), 64.8±2.9%, were lower (P=0.02) than those draining central brain regions (when averaging ROI #4–6), 70.2±3.3%, which agrees with previous literature in adults (20,28,29).

In posterior SSS (ROI #3 for aTRUPC), Y_v values measured by aTRUPC showed excellent agreement with global Y_v measured by TRUST, which were 63.6±3.5% and 62.2±2.2%, respectively. A paired t-test found no significant difference between the Y_v values measured by the two methods (P=0.25).

Y_v maps of all 4 neonates are shown in Figure 6b. It can be seen that the image quality is generally satisfactory and all major veins can be discerned.

DISCUSSION

This study presented a new sequence, termed aTRUPC, to measure cerebral venous oxygenation in neonates without using any exogenous contrast agent in scan duration of less than 4 minutes. The present study has several novel aspects. First, to our knowledge, the present study is the first to report measurement of central brain Y_v values in neonates. Prior studies were unable to measure Y_v in deep venous system because most MRI techniques such as TRUST (11), phase susceptometry (10), and T2-TRIR (12) can only measure global venous oxygenation in the superior sagittal sinus while near infrared methods (7–9) do not have the penetration depth to image deep veins. Another novel aspect is that the present study was conducted on healthy neonatal subjects in research-dedicated scan sessions. Most prior neonatal studies were performed on sick neonates and the research sequences were conducted as add-ons to clinical sequences. This is because it is challenging to recruit healthy neonates who would otherwise not undergo MRI to participate in MRI research studies. On the other hand, the benefit of recruiting healthy neonates for research-dedicated sessions is that we will have sufficient scan time to conduct systematic testing of the pulse sequence in terms of key imaging parameters, such as TFE factor, slice thickness, and VENC. Another benefit is that there will not be confounding factors due to pathology and

the measured results will truly represent normative values. Therefore, in this study, we took the effort to recruit healthy neonates, which made the above-mentioned technical development and optimization feasible. The importance of having a research-dedicated session is further underscored by the fact that, in our institution and in many other institutions around the world, neonates of several days old are scanned in natural sleep without using sedation. Therefore, this factor further limits the scan time available in this special population that is highly susceptible to motion, and our study design of a research MRI session is a worthy effort.

Cerebral oxidative metabolism plays a critical role in the rapidly developing neonatal brain. The complex structural and functional maturation processes place high demands on energy supply, which is manifested by the fast increase in cerebral metabolic rate of oxygen ($CMRO_2$) during this stage (7,11,12,30). Abnormal cerebral oxygen metabolism has been associated with various neonatal injuries and diseases. With recent advances of MRI, quantitative measurement of cerebral oxygen metabolism has shown clinical utility in several neonatal diseases. For instance, decreased $CMRO_2$ has been shown in neonates with CHD by two independent studies (10,13), and has also been demonstrated in neonates with PWML (15). Neonates with HIE have been reported to have lower oxygen extraction fraction than normal controls (12,14). Despite the success of these prior studies, they were largely based on global measurement of cerebral oxygen metabolism. Regional measurement of Y_v and $CMRO_2$ may provide additional important clinical values in neonatal care for a variety of reasons. First, early brain development has been shown to be heterogeneous in newborns. For example, using arterial spin labelling (ASL) perfusion MRI, Ouyang et al. found that the rate of cerebral blood flow (CBF) increase is significantly higher in the frontal lobe than in the occipital lobe (17). De Vis et al. studied regional perfusion values obtained with ASL as a function of postmenstrual age, and reported that relative regional CBF was the highest in the basal ganglia and thalamus at all time-points (18). Combined with regional CBF measures, regional Y_v measurement can provide better characterization of spatial patterns of oxygen consumption in neonates, thus improving our understanding of early human brain development. Second, many neonatal brain disorders are known to affect specific brain regions. For instance, the basal ganglia and thalamus are known to be more susceptible to damages in HIE (1,2). Another example is perinatal arterial ischemic stroke, and De Vis et al. reported that cerebral oxygen saturation was higher in the infarcted hemisphere than the contralateral hemisphere (31). The ability to measure regional Y_v will provide new insights into the disease pathology and guide therapy on an individual basis. In fact, even in healthy neonates, we have observed that veins draining cortical brain have lower Y_v values than veins draining central brain regions. This finding was consistent with previous reports in adults (20,28,29) and was thought to relate to the higher perfusion or CBF in the central brain regions compared to the cortices (32–34).

We note that the measurement of Y_v in aTRUPC is vessel-specific. To compute regional $CMRO_2$ from aTRUPC Y_v measurements, one needs to know the regional CBF that corresponds to the target veins. One feasible approach suggested by Fan et al. (35) is to use ASL to acquire quantitative CBF maps, and calculate the mean CBF values of ROIs placed in the brain regions drained by the target veins, then the regional $CMRO_2$ can be calculated using the Fick's principle (36).

In the last decade, techniques that combine T_2 preparation with fast readout schemes have been proposed to measure T_2 in organs with intensive motion or in less cooperative patients. T_2-prepared TFE or balanced steady-state free precession (bSSFP) have been used for T_2 mapping of myocardium (22,37) and carotid artery vessel wall (38). Recently, T_2-prepared bSSFP was used to quantify the blood T_2 and oxygenation in umbilical vein of fetuses (39). The major difference of aTRUPC compared to these techniques is the employment of phase-contrast to separate out blood signal from surrounding tissues, which minimizes partial volume effect in blood T_2 estimation. In terms of acceleration, there have been reports using single-shot echo-planar imaging (EPI) for phase-contrast imaging of relatively large vessels such as aorta (40), carotid arteries (41), or SSS (42) in adults. However, the low in-plane spatial resolution of single-shot EPI makes it impractical to image small veins such as the internal cerebral veins, especially in neonates. Single-shot turbo spin echo has been widely used in clinical practice for fast imaging, however, the mixing among signal pathways with different motion-induced phases of the flowing blood (43) makes it unsuitable for phase-contrast imaging of the cerebral veins.

Besides T_2-based methods (20,44,45), MR susceptometry (35) and quantitative BOLD (46,47) have also been exploited to measure regional Y_v. For example, Fan et al. (35) proposed a susceptibility-based approach to measure Y_v in vein segments that approximate a long cylinder parallel to B_0. One advantage of this technique is that it employs standard gradient-echo sequence and is therefore readily applicable on clinical MR scanners. However, its restriction on the orientation and shape of veins makes it not suitable for studying the tortuous deep veins which mainly fall in the anterior-posterior direction that is perpendicular to B_0. In contrast, aTRUPC has no such restriction and can measure the veins in any shape and orientations when proper flow-encoding direction is chosen. The quantitative BOLD method (46,47) requires long scan duration which is impractical in neonates.

There are a few limitations in the presented work. First, the Y_v map obtained in this study is 2D in nature. Further expansion of the technique to 3D acquisitions would require additional acceleration techniques such as compressed sensing (48). Second, although we have shortened the duration of the sequence to 3min 44s, motion could still occur during this time frame. Thus, further technical development should consider the implementation of motion correction schemes to the sequence, which will greatly improve its clinical applicability in neonates. Third, the hematocrit of the neonates was assumed to be 0.42 in this study, in future applications of this technique, hematocrit should be measured individually to account for potentially abnormal hematocrit levels in sick or premature neonates. Fourth, in the present study, we did not optimize the recovery time after post-saturation in this study. Although numerical simulation suggested that a recovery time of 1000ms is a good trade-off between aTRUPC signal and susceptibility to motion, future experiments should be performed to validate this selection. Finally, clinical utility of the proposed technique in pathological conditions, especially those specifically affecting deep brain structures, should be established in future work.

CONCLUSION

We developed a non-invasive MRI technique, aTRUPC, to quantify Y_v in cortical and deep cerebral veins in neonates. The sequence was optimized in terms of sensitivity and accuracy of the underlying T_2 measurement. The scan time of the final protocol was less than 4 minutes and, using this protocol, normative venous oxygenation values for major cerebral veins were determined. aTRUPC MRI has the potential to provide vessel-specific quantification of Y_v in neonates.

Supplementary Material

Refer to Web version on PubMed Central for supplementary material.

Grant Sponsors:

NIH R01 NS109029, R01 NS106702, R01 NS106711, R01 MH084021, R21NS100006, R21 NS095342, P41 EB015909.

REFERENCES

1. Douglas-Escobar M, Weiss MD. Hypoxic-ischemic encephalopathy: a review for the clinician. JAMA Pediatr 2015;169(4):397–403. [PubMed: 25685948]
2. de Vries LS, Groenendaal F. Patterns of neonatal hypoxic-ischaemic brain injury. Neuroradiology 2010;52(6):555–566. [PubMed: 20390260]
3. van der Aa NE, Benders MJ, Groenendaal F, de Vries LS. Neonatal stroke: a review of the current evidence on epidemiology, pathogenesis, diagnostics and therapeutic options. Acta Paediatr 2014;103(4):356–364. [PubMed: 24428836]
4. Peng SL, Dumas JA, Park DC, Liu P, Filbey FM, McAdams CJ, Pinkham AE, Adinoff B, Zhang R, Lu H. Age-related increase of resting metabolic rate in the human brain. NeuroImage 2014;98:176–183. [PubMed: 24814209]
5. Mintun MA, Raichle ME, Martin WR, Herscovitch P. Brain oxygen utilization measured with O-15 radiotracers and positron emission tomography. Journal of nuclear medicine : official publication, Society of Nuclear Medicine 1984;25(2):177–187.
6. Altman DI, Perlman JM, Volpe JJ, Powers WJ. Cerebral oxygen metabolism in newborns. Pediatrics 1993;92(1):99–104. [PubMed: 8516092]
7. Roche-Labarbe N, Carp SA, Surova A, Patel M, Boas DA, Grant PE, Franceschini MA. Noninvasive optical measures of CBV, StO(2), CBF index, and rCMRO(2) in human premature neonates' brains in the first six weeks of life. Hum Brain Mapp 2010;31(3):341–352. [PubMed: 19650140]
8. Dehaes M, Aggarwal A, Lin PY, Rosa Fortuno C, Fenoglio A, Roche-Labarbe N, Soul JS, Franceschini MA, Grant PE. Cerebral oxygen metabolism in neonatal hypoxic ischemic encephalopathy during and after therapeutic hypothermia. J Cereb Blood Flow Metab 2014;34(1):87–94. [PubMed: 24064492]
9. Durduran T, Zhou C, Buckley EM, Kim MN, Yu G, Choe R, Gaynor JW, Spray TL, Durning SM, Mason SE, Montenegro LM, Nicolson SC, Zimmerman RA, Putt ME, Wang J, Greenberg JH, Detre JA, Yodh AG, Licht DJ. Optical measurement of cerebral hemodynamics and oxygen metabolism in neonates with congenital heart defects. J Biomed Opt 2010;15(3):037004. [PubMed: 20615033]
10. Jain V, Buckley EM, Licht DJ, Lynch JM, Schwab PJ, Naim MY, Lavin NA, Nicolson SC, Montenegro LM, Yodh AG, Wehrli FW. Cerebral oxygen metabolism in neonates with congenital heart disease quantified by MRI and optics. Journal of cerebral blood flow and metabolism : official journal of the International Society of Cerebral Blood Flow and Metabolism 2014;34(3):380–388.

11. Liu P, Huang H, Rollins N, Chalak LF, Jeon T, Halovanic C, Lu H. Quantitative assessment of global cerebral metabolic rate of oxygen (CMRO2) in neonates using MRI. NMR in biomedicine 2014;27(3):332–340. [PubMed: 24399806]
12. De Vis JB, Petersen ET, Alderliesten T, Groenendaal F, de Vries LS, van Bel F, Benders MJ, Hendrikse J. Non-invasive MRI measurements of venous oxygenation, oxygen extraction fraction and oxygen consumption in neonates. NeuroImage 2014;95:185–192. [PubMed: 24685437]
13. Ferradal SL, Stout JN, Gagoski B, Vyas R, Ha C, Bolar DS, Cheng HH, Newburger J, Franceschini MA, Adalsteinsson E, Grant PE. Optimizing Unanesthetized Cerebral Oxygen Consumption Measures: Comparison of NIRS and MRI Approaches in Neonates with Congenital Heart Disease. OSA Technical Digest (online); 2016 2016/04/25; Fort Lauderdale, Florida. Optical Society of America. p OM4C.6. (OSA Technical Digest (online)).
14. Shetty AN, Lucke AM, Liu P, Sanz Cortes M, Hagan JL, Chu ZD, Hunter JV, Lu H, Lee W, Kaiser JR. Cerebral oxygen metabolism during and after therapeutic hypothermia in neonatal hypoxic-ischemic encephalopathy: a feasibility study using magnetic resonance imaging. Pediatr Radiol 2018.
15. Qi Y, Liu P, Lin Z, Lu H, Wang X. Hemodynamic and Metabolic Assessment of Neonates With Punctate White Matter Lesions Using Phase-Contrast MRI and T2-Relaxation-Under-Spin-Tagging (TRUST) MRI. Frontiers in physiology 2018;9:233. [PubMed: 29615927]
16. Lin PY, Roche-Labarbe N, Dehaes M, Fenoglio A, Grant PE, Franceschini MA. Regional and hemispheric asymmetries of cerebral hemodynamic and oxygen metabolism in newborns. Cereb Cortex 2013;23(2):339–348. [PubMed: 22328446]
17. Ouyang M, Liu P, Jeon T, Chalak L, Heyne R, Rollins NK, Licht DJ, Detre JA, Roberts TPL, Lu H, Huang H. Heterogeneous increases of regional cerebral blood flow during preterm brain development: Preliminary assessment with pseudo-continuous arterial spin labeled perfusion MRI. Neuroimage 2017;147:233–242. [PubMed: 27988320]
18. De Vis JB, Petersen ET, de Vries LS, Groenendaal F, Kersbergen KJ, Alderliesten T, Hendrikse J, Benders MJ. Regional changes in brain perfusion during brain maturation measured non-invasively with Arterial Spin Labeling MRI in neonates. Eur J Radiol 2013;82(3):538–543. [PubMed: 23199750]
19. Ferriero DM. Neonatal brain injury. N Engl J Med 2004;351(19):1985–1995. [PubMed: 15525724]
20. Krishnamurthy LC, Liu P, Ge Y, Lu H. Vessel-specific quantification of blood oxygenation with T2-relaxation-under-phase-contrast MRI. Magn Reson Med 2014;71(3):978–989. [PubMed: 23568830]
21. Krishnamurthy LC, Mao D, King KS, Lu H. Correction and optimization of a T2-based approach to map blood oxygenation in small cerebral veins. Magn Reson Med 2016;75(3):1100–1109. [PubMed: 25846113]
22. Ding H, Fernandez-de-Manuel L, Schar M, Schuleri KH, Halperin H, He L, Zviman MM, Beinart R, Herzka DA. Three-dimensional whole-heart T2 mapping at 3T. Magn Reson Med 2015;74(3):803–816. [PubMed: 25242141]
23. Li C, Magland JF, Zhao X, Seifert AC, Wehrli FW. Selective in vivo bone imaging with long-T2 suppressed PETRA MRI. Magn Reson Med 2017;77(3):989–997. [PubMed: 26914767]
24. Brown RW, Haacke EM, Cheng YCN, Thompson MR, Venkatesan R. Magnetic resonance imaging: physical principles and sequence design. Hoboken, New Jersey: John Wiley & Sons; 2014 448–468 p.
25. Liu P, Chalak LF, Krishnamurthy LC, Mir I, Peng SL, Huang H, Lu H. T1 and T2 values of human neonatal blood at 3 Tesla: Dependence on hematocrit, oxygenation, and temperature. Magn Reson Med 2016;75(4):1730–1735. [PubMed: 25981985]
26. Jenkinson M, Bannister P, Brady M, Smith S. Improved optimization for the robust and accurate linear registration and motion correction of brain images. Neuroimage 2002;17(2):825–841. [PubMed: 12377157]
27. Okell TW, Chappell MA, Kelly ME, Jezzard P. Cerebral blood flow quantification using vessel-encoded arterial spin labeling. J Cereb Blood Flow Metab 2013;33(11):1716–1724. [PubMed: 23921895]

28. Jain V, Magland J, Langham M, Wehrli FW. High temporal resolution in vivo blood oximetry via projection-based T2 measurement. Magn Reson Med 2013;70(3):785–790. [PubMed: 23081759]
29. Mao D, Li Y, Liu P, Peng SL, Pillai JJ, Lu H. Three-dimensional mapping of brain venous oxygenation using R2* oximetry. Magn Reson Med 2018;79(3):1304–1313. [PubMed: 28585238]
30. Yoxall CW, Weindling AM. Measurement of cerebral oxygen consumption in the human neonate using near infrared spectroscopy: cerebral oxygen consumption increases with advancing gestational age. Pediatr Res 1998;44(3):283–290. [PubMed: 9727702]
31. De Vis JB, Petersen ET, Kersbergen KJ, Alderliesten T, de Vries LS, van Bel F, Groenendaal F, Lemmers PM, Hendrikse J, Benders MJ. Evaluation of perinatal arterial ischemic stroke using noninvasive arterial spin labeling perfusion MRI. Pediatr Res 2013;74(3):307–313. [PubMed: 23797533]
32. Perlmutter JS, Powers WJ, Herscovitch P, Fox PT, Raichle ME. Regional asymmetries of cerebral blood flow, blood volume, and oxygen utilization and extraction in normal subjects. J Cereb Blood Flow Metab 1987;7(1):64–67. [PubMed: 3492507]
33. Hatazawa J, Fujita H, Kanno I, Satoh T, Iida H, Miura S, Murakami M, Okudera T, Inugami A, Ogawa T, et al. Regional cerebral blood flow, blood volume, oxygen extraction fraction, and oxygen utilization rate in normal volunteers measured by the autoradiographic technique and the single breath inhalation method. Ann Nucl Med 1995;9(1):15–21. [PubMed: 7779525]
34. Nakane H, Ibayashi S, Fujii K, Sadoshima S, Irie K, Kitazono T, Fujishima M. Cerebral blood flow and metabolism in patients with silent brain infarction: occult misery perfusion in the cerebral cortex. J Neurol Neurosurg Psychiatry 1998;65(3):317–321. [PubMed: 9728942]
35. Fan AP, Benner T, Bolar DS, Rosen BR, Adalsteinsson E. Phase-based regional oxygen metabolism (PROM) using MRI. Magn Reson Med 2012;67(3):669–678. [PubMed: 21713981]
36. Kety SS, Schmidt CF. The Effects of Altered Arterial Tensions of Carbon Dioxide and Oxygen on Cerebral Blood Flow and Cerebral Oxygen Consumption of Normal Young Men. J Clin Invest 1948;27(4):484–492. [PubMed: 16695569]
37. Huang TY, Liu YJ, Stemmer A, Poncelet BP. T2 measurement of the human myocardium using a T2-prepared transient-state TrueFISP sequence. Magn Reson Med 2007;57(5):960–966. [PubMed: 17457877]
38. Coolen BF, Poot DH, Liem MI, Smits LP, Gao S, Kotek G, Klein S, Nederveen AJ. Three-dimensional quantitative T1 and T2 mapping of the carotid artery: Sequence design and in vivo feasibility. Magn Reson Med 2016;75(3):1008–1017. [PubMed: 25920036]
39. Rodriguez-Soto AE, Langham MC, Abdulmalik O, Englund EK, Schwartz N, Wehrli FW. MRI quantification of human fetal O2 delivery rate in the second and third trimesters of pregnancy. Magn Reson Med 2018;80(3):1148–1157. [PubMed: 29359353]
40. Guilfoyle DN, Gibbs P, Ordidge RJ, Mansfield P. Real-time flow measurements using echo-planar imaging. Magn Reson Med 1991;18(1):1–8. [PubMed: 2062222]
41. Firmin DN, Klipstein RH, Hounsfield GL, Paley MP, Longmore DB. Echo-planar high-resolution flow velocity mapping. Magn Reson Med 1989;12(3):316–327. [PubMed: 2628682]
42. Lin Z, Li Y, Su P, Mao D, Wei Z, Pillai JJ, Moghekar A, van Osch M, Ge Y, Lu H. Non-contrast MR imaging of blood-brain barrier permeability to water. Magn Reson Med 2018;80(4):1507–1520. [PubMed: 29498097]
43. Storey P, Atanasova IP, Lim RP, Xu J, Kim D, Chen Q, Lee VS. Tailoring the flow sensitivity of fast spin-echo sequences for noncontrast peripheral MR angiography. Magn Reson Med 2010;64(4):1098–1108. [PubMed: 20725934]
44. Guo J, Wong EC. Venous oxygenation mapping using velocity-selective excitation and arterial nulling. Magn Reson Med 2012;68(5):1458–1471. [PubMed: 22294414]
45. Bolar DS, Rosen BR, Sorensen AG, Adalsteinsson E. QUantitative Imaging of eXtraction of oxygen and TIssue consumption (QUIXOTIC) using venular-targeted velocity-selective spin labeling. Magn Reson Med 2011;66(6):1550–1562. [PubMed: 21674615]
46. He X, Yablonskiy DA. Quantitative BOLD: mapping of human cerebral deoxygenated blood volume and oxygen extraction fraction: default state. Magn Reson Med 2007;57(1):115–126. [PubMed: 17191227]

47. Lee H, Englund EK, Wehrli FW. Interleaved quantitative BOLD: Combining extravascular R2' - and intravascular R2-measurements for estimation of deoxygenated blood volume and hemoglobin oxygen saturation. Neuroimage 2018;174:420–431. [PubMed: 29580967]

48. Lustig M, Donoho D, Pauly JM. Sparse MRI: The application of compressed sensing for rapid MR imaging. Magn Reson Med 2007;58(6):1182–1195. [PubMed: 17969013]

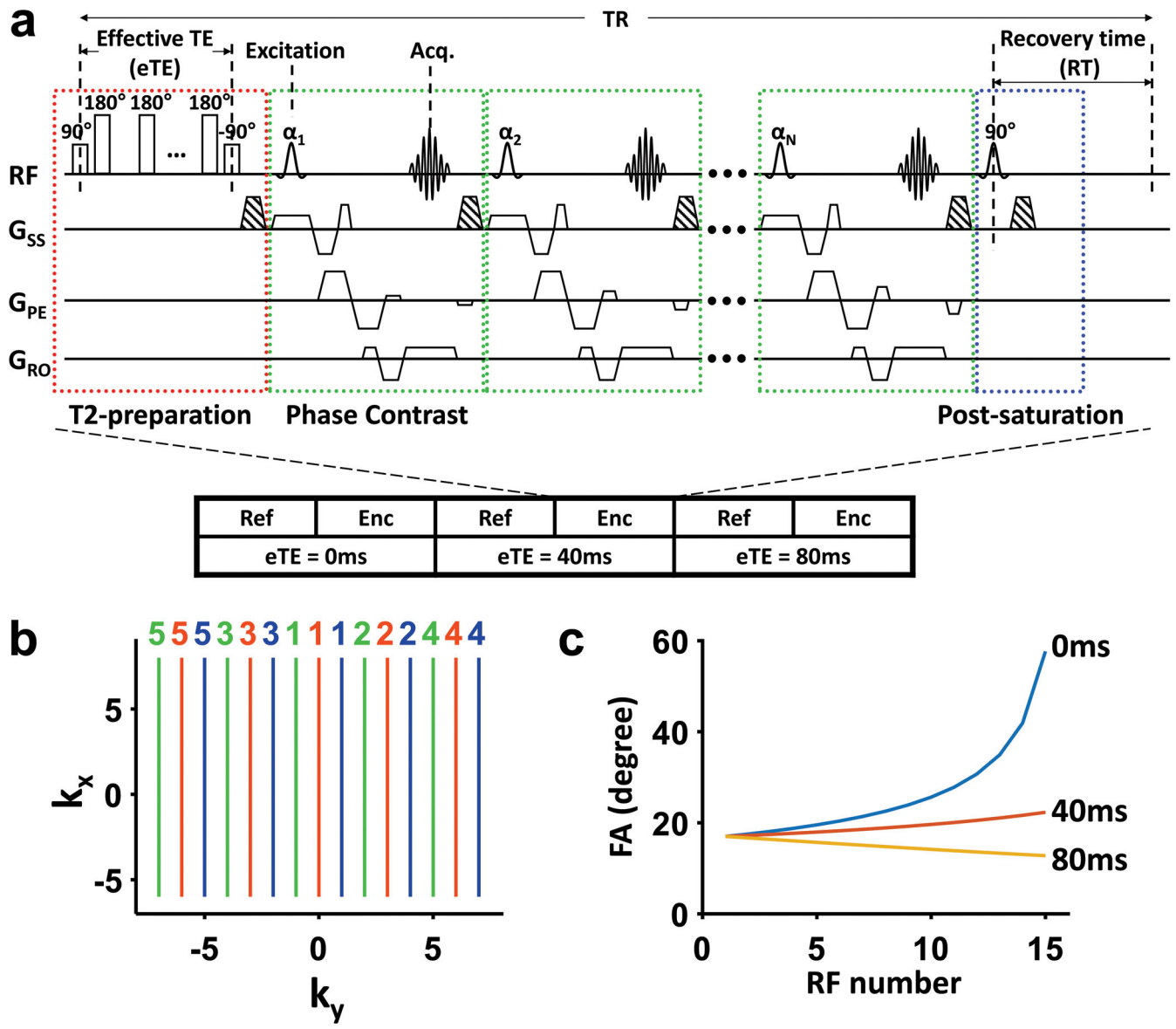

Figure 1.

Illustration of the aTRUPC pulse sequence. (a) The pulse sequence consists of three components: T_2-preparation (red box), TFE phase-contrast acquisition modules (green boxes) and post-saturation (blue box). The phase-contrast module separates flowing blood signal from static tissues through complex subtraction of phase reference ("ref" in the illustration) and velocity-encoded ("enc" in the illustration) images. Note that for flow-encoding along phase-encoding direction, the slice and readout directions are flow-compensated while the phase-encoding direction is flow-encoded. α_i (i = 1, 2, …, N, where N is the TFE factor) represents the flip angle of each acquisition module. T_2-preparation with varying duration (0ms, 40ms, and 80ms) is applied to modulate the T2-weighting. Spin history of each TR is minimized through post-saturation pulse. The striped trapezoids indicate spoiler gradients. (b) Illustration of the centric view ordering scheme. k-Space lines acquired in the same TR are represented by the same color. The colored numbers beside the

k-space lines indicate the order in which these lines are acquired within each TR. Lines closest to the center of k-space are sampled at the very beginning of the acquisition train immediately after T_2-preparation, while the peripheral lines are acquired later. (c) Variable FA series of each eTE with TFE factor of 15. Note that the first FA is the same for all eTEs.

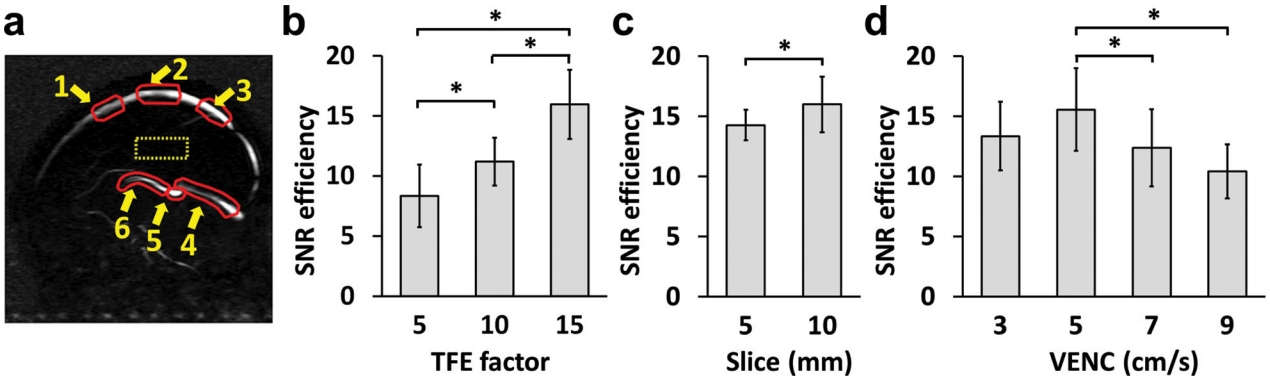

Figure 2.

Dependence of SNR efficiency on sequence parameters in neonates. (a) Illustration of ROIs on a CD image. Red contours represent the preliminary ROIs to quantify blood signal at 6 different locations. The yellow dashed box shows the ROI to estimate residual tissue signal. (b) Comparison of SNR efficiency, quantified by blood/tissue/$\sqrt{\text{scan time}}$, across TFE factors. (c) Comparison of SNR efficiency across slice thicknesses. (d) Comparison of SNR efficiency across VENC values. For each subject, the SNR efficiency values were averaged across the 6 ROIs. Error bars indicate standard deviations across subjects.

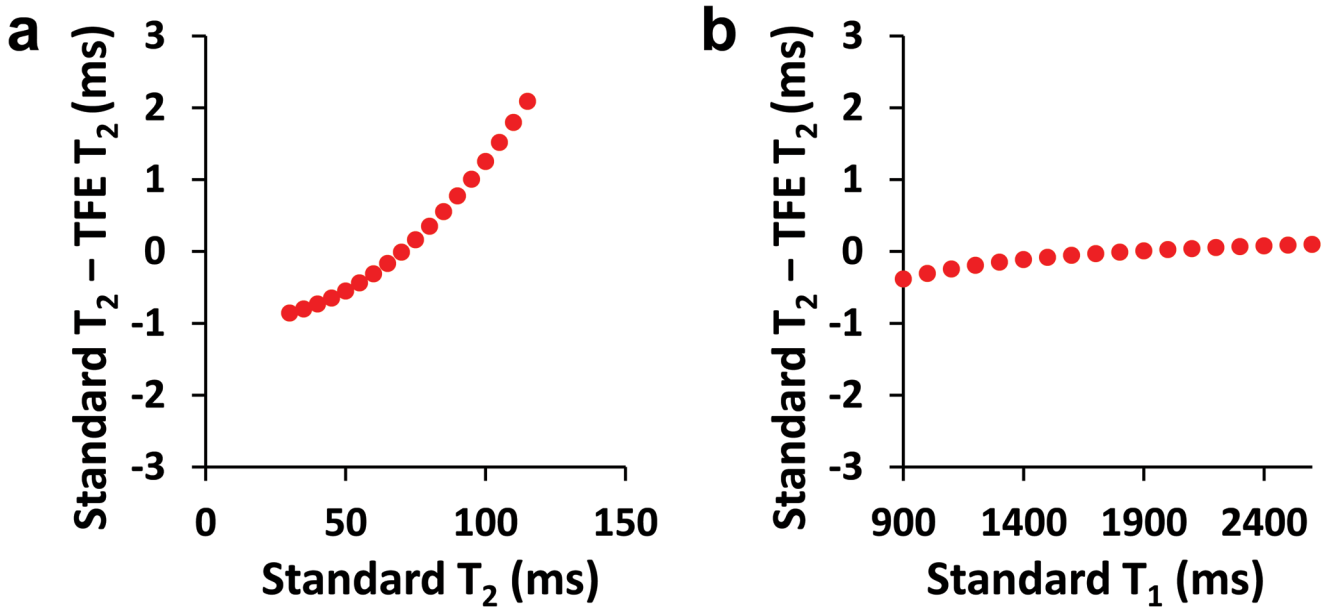

Figure 3.

Numerical simulation results of the difference between TFE-T_2 and standard T_2 as a function of standard T_1 and T_2 values. (a) The difference as a function of T_2. T_1 was fixed and was assumed to be 1800ms. (b) The difference as a function of T_1. T_2 was fixed and was assumed to be 70ms.

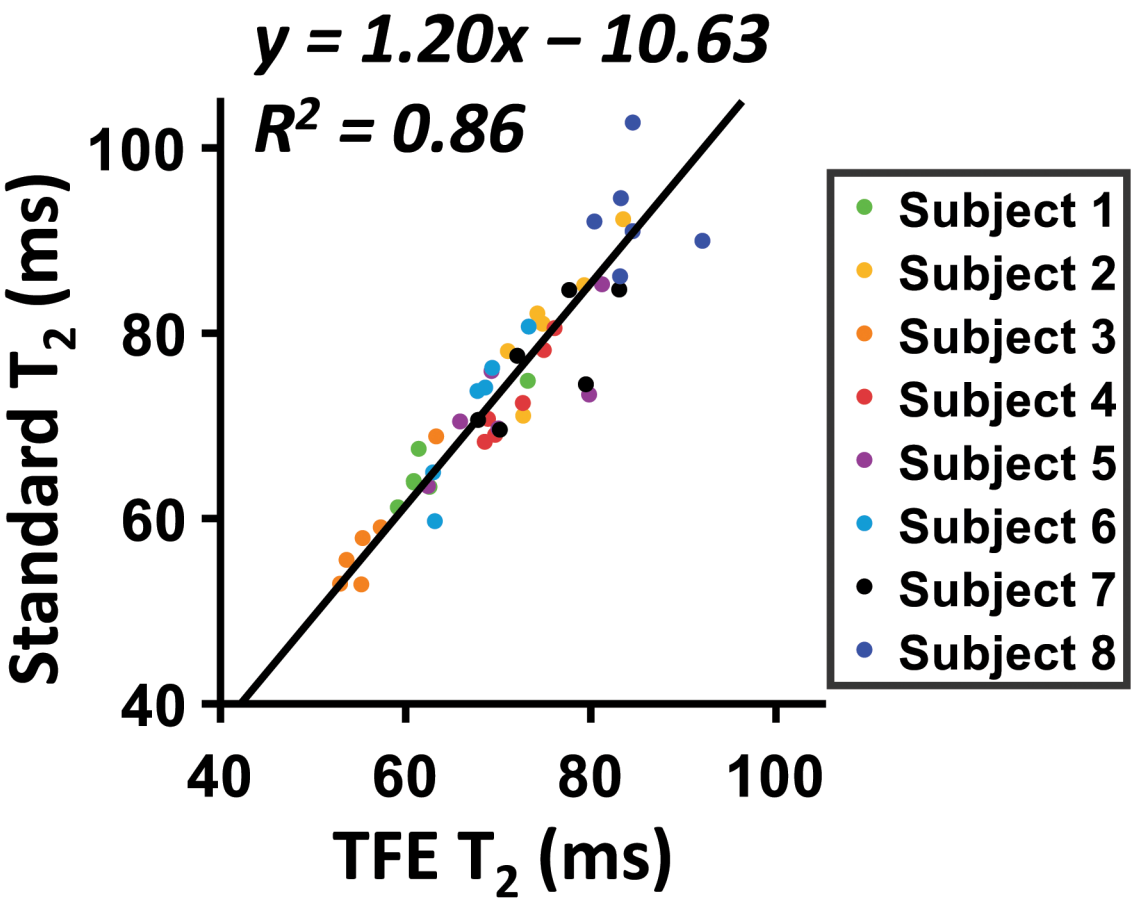

Figure 4.

Scatter plot between TFE-T_2 measured by aTRUPC and standard T_2 measured by original TRUPC. Each dot represents T_2 of one ROI on one subject. Solid line indicates the fitting curve. Dashed line indicates the identity line.

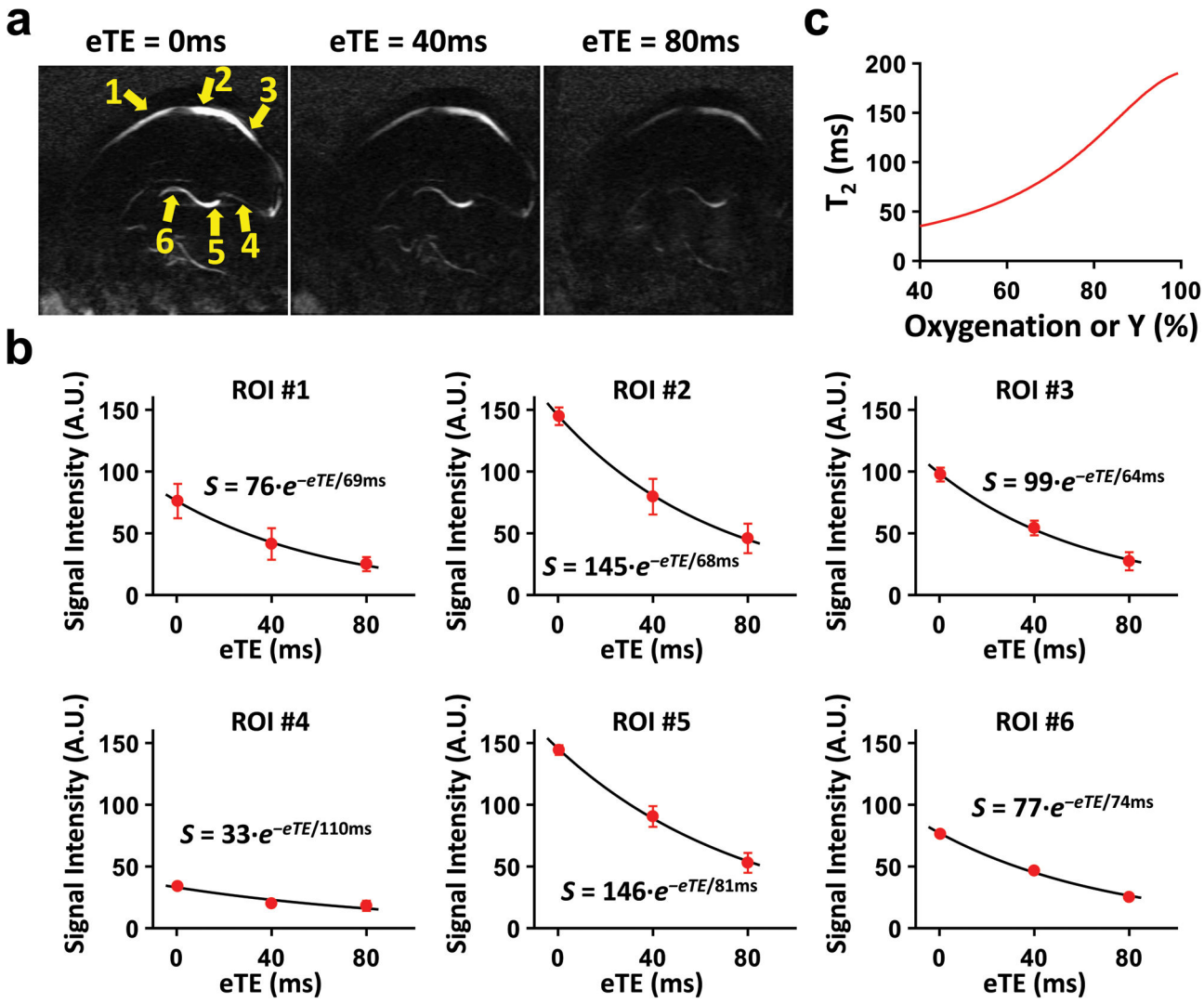

Figure 5.

Data from a complete aTRUPC scan in a representative neonate. (a) Averaged CD images at 3 eTEs. The yellow arrows show the ROIs from which the data in (b) were derived. (b) CD signals as a function of eTEs in each ROI. The solid curves show the fitted results, and error bars indicate the standard deviation of CD signals across the 4 repetitions. The fitted equations are also shown. (c) The neonate-specific calibration plot, shown here for a hematocrit of 0.42.

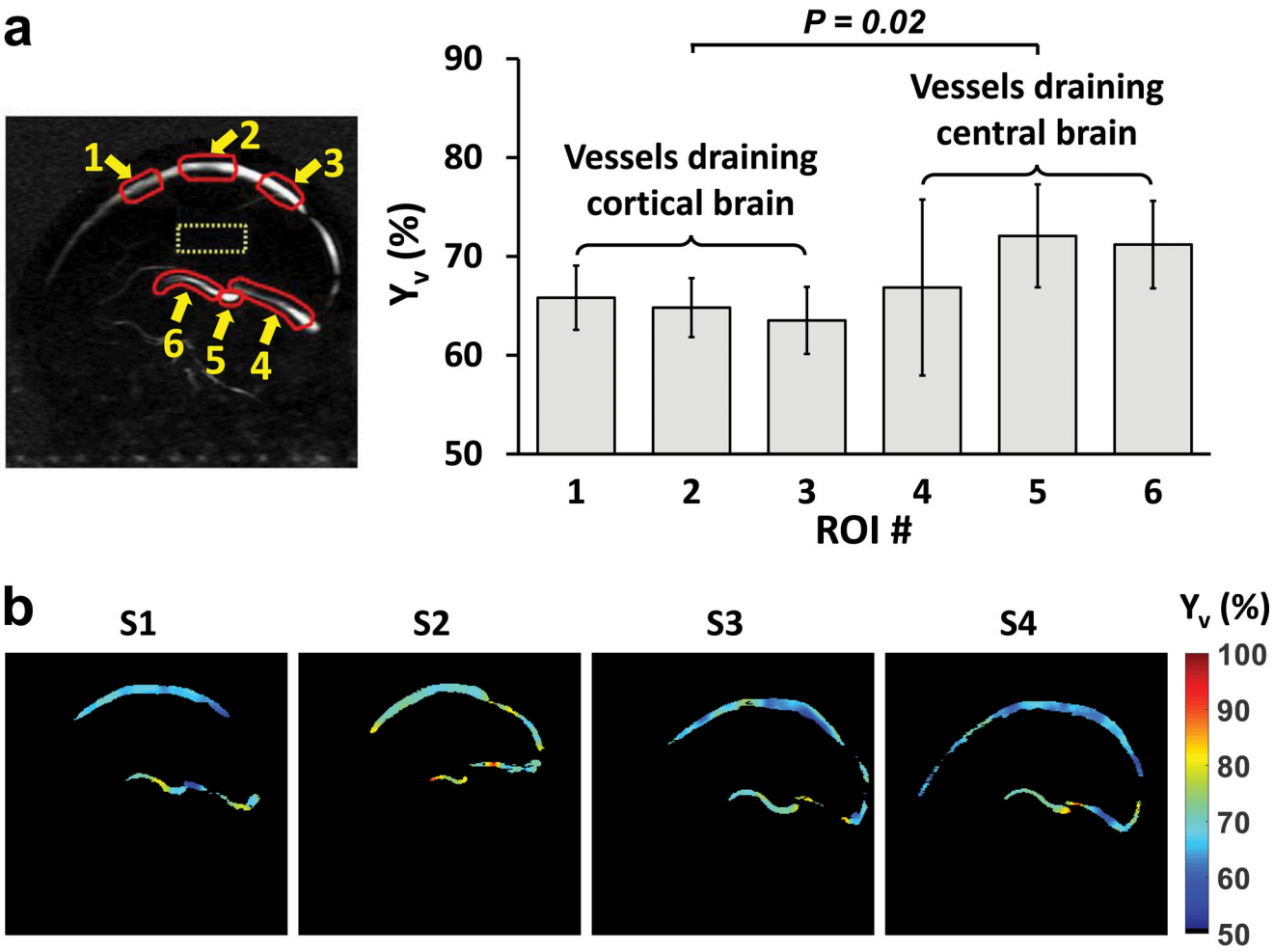

Figure 6.

Summary of aTRUPC results in healthy neonates. (a) Group-averaged Y_v of each ROI. Error bars indicate standard deviations across subjects. (a) Y_v maps of the 4 neonates (labeled as S1 to S4).